Optoelectronic synapses using vertically aligned graphene/diamond heterojunctions

Y. Mizuno, Y. Ito, and *K. Ueda

Graduate School of Engineering, Nagoya University

Furo-cho, Chikusa-ku, Nagoya 464-8603, Japan

Abstract

The present work demonstrates that vertically aligned graphene (VG)/diamond heterojunctions can function as optoelectronically-controllable synapses, which are connection parts of neurons and key elements for the memory functions of human brain. These junctions mimic several of the fundamental characteristics of biological synapses, including producing an excitatory postsynaptic current (EPSC), exhibiting a transition from short-term memory (STM) to long-term memory (LTM) states, and paired pulse facilitation (PPF), all of which are optically controllable. These junctions also exhibit photo-sensing properties and photo-controllable synaptic plasticity, meaning that they have similar functions as occur in the human brain and retina. Arrays fabricated from these junctions were found to function as image sensors that could provide an optical memory function and selectively memorize information depending on the relative importance of the data. These results are expected to assist in the realization of neuromorphic optical computers simulating human visual memory systems that are modulated by specific interests.

Keywords: graphene, diamond, synapse, brain, optically-controllable
*Corresponding author. Tel: +81-52-789-3567. E-mail: k-ueda@numse.nagoya-u.ac.jp

1. Introduction

Modern information society is based on various computing devices consisting of integrated circuits using semiconductors, which process vast quantities of data. Present day computers employ von Neumann architecture, in which the computing and storage units are physically separated and data are processed sequentially in each unit. As such, it is necessary to frequently transfer many data between processors and memory units, and these data are frequently blocked along these transfer paths. This problem, representing the so-called von Neumann bottleneck, is the most important factor currently limiting the processing speed and energy efficiency of Neumann-type computers [1].

One promising approach to overcoming the limitations of Neumann-type computers is the use of neuromorphic architectures [2, 3] that simulate the neural systems in the human brain. In the brain, complicated processes such as image recognition are massively parallel processed while consuming only a small amount of power (on the order of 10 W) [4]. The human brain contains an enormous number of neurons connected by synapses. Synaptic plasticity, which is the change in signal transfer efficiency via synapses caused by dynamic variations in synaptic strength as a result of stimulation, is considered to be vital to memory and learning. Many researchers have attempted to reproduce synaptic functions using transistors [5], phase-change memories [6] and memristors [7]. The latter are passive devices having multiple, nonvolatile resistance states, and have frequently been used to fabricate neuromorphic systems because their analog resistance change and nonvolatile memory functions are believed to mimic synaptic plasticity [8-10].

Recently, photocontrollable memristors (photomemristors) representing an evolved type of memristor having optically-controllable nonvolatile resistance states have been reported [11-14]. Photomemristors provide both photo-detection and non-volatile

memory functions in a single device, and could potentially be used to produce novel neuromorphic optical memory devices with functions similar to both human memory and visual perception. Very recently, several photomemristor heterostructures comprising oxides [15-18], transition metal dichalcogenides (TMDs) [19, 20] and Si nanomembranes [21] have been found to function as optoelectronic synapses exhibiting photo-sensing properties and mimicking synaptic plasticity. However, the study of artificial optoelectronic synapses is a new field and the search for novel materials with optoelectronic synaptic functions and optical applications continues [22]. Our own group has studied the unique physical properties of graphene/diamond (involving sp^2-sp^3 carbon interfaces), and we have demonstrated VG/diamond junctions became photomemristors [14, 23]. The junctions have also exhibited multibit photomemory functions that originate from their high responsivity to optical pulses [24].

The present study demonstrates that VG/diamond heterojunctions can be used as optoelectronic synapses that exhibit some of the basic functions of the human brain, such as an EPSC, synaptic plasticity (with a transition from STM to LTM) and PPF. We also report the construction of arrays of VG/diamond junctions that can be used as novel image sensors with optoelectronic memory functions.

2. Experimental Section

Semiconducting diamond films lightly doped with B were homoepitaxially grown on diamond (100) substrates by microwave plasma CVD [25]. VG layers (that is, carbon nanowalls) were grown *in situ* on the B-doped semiconducting diamond layers in the same CVD apparatus. Details of the fabrication of the VG/diamond bilayers have been

described in a previous paper [23]. Junctions with diameters of 80-160 μm were fabricated using the VG/diamond bilayers [23, 24]. The *I-V* characteristics of these junctions in response to photoirradiation were measured using blue light emitting diodes (LEDs) or a fluorescent lamp in air at room temperature. Raman spectra of the junctions in either the high resistance states (HRS) or low resistance states (LRS) were acquired by fabricating specimens in which Ni upper electrodes were slightly shifted to leave a small area of each VG/diamond surface uncovered by the electrode. Raman spectra were obtained from each VG/diamond surface at a region very close to the edge of the Ni electrode immediately after applying a bias and in conjunction with photoirradiation, to examine the difference between the HRS and LRS. These Raman spectra were measured at an excitation wavelength of 532 nm.

3. Results and Discussion

The current-voltage (*I-V*) characteristics of these junctions were measured under photoirradiation (Figs. 1a and 1b, inset) at the maximum voltage (±8 V) for approximately 10 s, using a fluorescent lamp. The *I-V* data exhibited hysteresis and indicated that a HRS was obtained upon photoirradiation together with a negative bias (-8 V), while a LRS was generated when applying a positive bias (+ 8 V). In contrast, the application of ±8 V under dark conditions did not induce a resistance change (Fig 1b). The retention properties of the junctions in HRS or LRS was examined (Fig. 1c). After changing to the HRS or LRS, the junction resistance was measured at a bias voltage of +2 V under dark conditions and negligibly small current changes (reflecting negligibly small resistance change of the junction) were observed for both the HRS and LRS. Lower measurement voltage of + 2

V was adopted to prevent unexpected resistivity change of the junctions. The resistance difference ratio between the HRS and LRS (= R_{HRS}/R_{LRS}) was approximately 10^2 and was maintained for 2 days. These results suggest that the junctions were able to act as photomemristors. In the case of normal memristors, the resistance state is changed only by an electronic stimulus such as a bias voltage [7], while the resistance state of a photomemristor can be controlled by photoirradiation, which is relatively rare [11-14]. Photomemristors can provide both photosensing and nonvolatile memory functions in a single device, and so are promising candidates for fabricating optically-controllable neuromorphic systems.

These VG/diamond photomemristors are believed to function as they do because of the redox reactions that occur at the graphene layers and/or the graphene/diamond (sp^2/sp^3 carbon) interfaces. Such reactions involve the migration of oxygen ions in response to photoirradiation and the application of a bias voltage [14, 23]. Specifically, the application of a negative bias voltage in conjunction with photoirradiation caused negatively-charged oxygen ions to move toward the graphene/diamond interfaces, such that the interfacial graphene layers were oxidized (Fig. 1c). The oxidized graphene layers (having a high proportion of sp^3 carbon) then behaved as insulating layers. This is not unexpected because it is well known that oxidation of graphene layers increases the proportion of sp^3 bonded carbons while reducing conductivity [26]. Conversely, the application of a positive bias during photoirradiation caused oxygen ions to migrate to the upper Ni electrodes, so that the interfacial graphene layers were reduced (meaning that they had a high concentration of sp^2 carbon) and became conductive. This sp^2-sp^3 transition of the interfacial graphene layers induced by the movement of oxygen ions is thought to play a major role in the photomemristive behavior of these devices. The mechanism described

above is supported by the observation that exposure of these devices to air for several days was necessary to obtain the memristive characteristics, and so the movement of electrically charged particles such as oxygen ions in response to a bias and photoirradiation was the primary factor driving the switching behavior. The junctions also showed light wavelength selectivity and only blue or purple light can induce the large conductivity change, which was also considered to be related to the photo-induced redox reactions of the graphene-diamond interfaces [14, 23]. Evidence for the proposed mechanism was also provided by the Raman data obtained for the VG/diamond junctions in the HRS and LRS (Fig. 1d). These spectra show typical features of VG/diamond bilayers as well as peaks related to vertically aligned graphene (G, 2D, D, and D′ peaks) [27, 28] and diamond (labeled as Dia.) [29]. The G and D peaks correspond to the stretching of C-C bonds in graphitic materials (that is, sp^2 carbon) and sp^3-like defects and/or edge formations in sp^2 structures, respectively [27]. Therefore, the ratio of the intensities of the D and G peaks (I_D/I_G) corresponds to the sp^3/sp^2 ratio in the graphene layers. The I_D/I_G ratios for the HRS and LRS were estimated to be 1.35 and 1.32, respectively. The higher I_D/I_G value for the HRS suggests an increase in the sp^3/sp^2 ratio in this state, in agreement with our suggestion that the oxidation (or reduction) of interfacial graphene [that is, increases in the proportion of sp^3 (or sp^2) carbon] plays a major role in driving the photomemristive behavior of these devices. The same trends were previously observed in the Raman spectra obtained from other VG/diamond junctions in the HRS and LRS that exhibited multibit optoelectronic memory functions [24]. These results indicate that the photomemristive behavior resulted from sp^2-sp^3 transitions induced by the movement of oxygen ions at the graphene/diamond interfaces, although direct evidence for this migration of oxygen will be necessary to support this

theory.

The VG/diamond junctions also exhibited clear responses to optical pulses and brain-like optoelectronic memory properties were observed. Figure 2a shows the effect of optical pulses with an intensity of 78 μW/cm^2, a pulse width of 50 ms and a frequency of 0.2 Hz by using blue LED on the junction current at a bias voltage of +8 V. This current, which depended on the conductivity of the junction, increased stepwise in response to each optical pulse, and a value of approximately 11 nA was obtained after applying 10 optical pulses. The current was subsequently maintained without significant deterioration. This generation of a current after frequent stimulation (via optical pulses in this case) is analogous to the generation of the EPSC at biological synapses [15, 16]. Thus, the present VG/diamond junctions can be said to have produced an EPSC in response to optical stimulation. The magnitude of the EPSC generated by the junctions could be tuned by varying the intensity, width, frequency and numbers of the optical pulses (Fig. 2a, inset), suggesting good controllability of the EPSC based on applying optical spikes. The energy consumption (E) per event under these conditions was estimated to be approximately 440 pJ using the equation $E = V_J \times I_J \times t$, where V_J is the bias voltage applied to the junction and I_J is the junction current during an optical spike with duration t. This energy value is quite low and suggests the possibility of fabricating devices that mimic brain functions with very low energy consumption.

The magnitude of the EPSC obtained from the junctions could be varied by adjusting the bias polarity followed by photoirradiation. Figure 2b plots the EPSC as a function of the number of optical pulses with a negative bias voltage (–8 V). Initially, the EPSC was produced by applying 20 optical pulses at a positive bias voltage (+8 V), after which an attempt was made to depress the EPSC by applying optical pulses in conjunction with a

negative bias voltage. The EPSC was found to systematically decrease as optical pulses were applied with this negative voltage, eventually becoming more than one order of magnitude smaller after 15 optical pulses. The EPSC of the junction was tuned after its generation, and the magnitude of the EPSC could later be decreased (or increased) by changing the bias polarity in conjunction with photoirradiation. These features correspond to the excitatory and inhibitory functions of synapses, and so these junctions are considered to have bias-tunable excitatory or inhibitory synaptic characteristics. The wide-rage bidirectional optical control of the resistance states by single light source (blue, ~470 nm) is one of significant features of the VG/diamond junctions. Considering the working principles of the junctions described above, the step-by-step increase (or decrease) of their conductivity corresponds to the stepwise reduction (or oxidation) of the interfacial graphene layers. The minimal energy consumption of the junctions is attributed to the small amount of energy required for the migration of oxygen ions through the graphene and/or the graphene/diamond interfaces. Clarification of the detailed mechanism of the synaptic behaviors will be a subject of future study by our group.

Figure 2c summarizes the effects of the number of optical pulses (either 3 or 12 pulses) on the conductance decay of the junctions, based on measuring conductance after applying various numbers of pulses (78 μW/cm^2, 50 ms width) at a bias voltage of +8 V. The conductance is seen to have gradually decreased over time, and this decay was evaluated using the formula [16, 30, 31]

$$\boldsymbol{G(t)/G_0 = exp\left[-(t/\tau)^{\beta}\right]}, \quad (1)$$

which is often used to analyze the loss of human memory. Here, $G(t)$ and G_0 are the conductance at measurement time t and just after applying the optical pulse, respectively, $G(t)/G_0$ is the normalized conductance, τ is the relaxation time for the conductance decay,

and β is an index with a value between 0 and 1. The conductance decay curves could be well fitted using this equation and τ was estimated to be 5.4 s for three pulses and 1558 s for 12 pulses (Fig. 2c). In this case, a long (short) τ indicates long (short) junction memory, and Fig. 2d demonstrates that τ was short up to approximately four pulses, gradually increased beginning at five pulses and then plateaued at approximately 1600 s above seven pulses. The τ value following seven or more pulses was close to three orders of magnitude greater than that for less than four pulses, confirming a transition to long-term memory. In addition, β increased from approximately 0.2 and plateaued at approximately 0.5 after nine pulses. A larger β value also corresponds to a reduced decay in these samples, and so the memory retention time for the VG/diamond junctions was evidently increased by increasing the quantity of optical pulses. Overall, these data confirm that the memory characteristics of the junctions could be modified by optical stimulation (that is, applying optical pulses), and a transition from STM to LTM states could be induced by using more intense optical stimulation. In the human brain, the STM – LTM transition is based on synaptic plasticity and is considered to be fundamental to the memory process [32]. Consequently, the appearance of an STM – LTM transition during these trials using the junctions indicates that these devices mimic optically controllable synaptic plasticity.

The STM–LTM transition could also be induced by tuning the frequency of the optical pulses, and Figs. 3a and 3b plot the junction current over time in response to optical pulse frequency values of 2 and 50 mHz, respectively. In the case of the 2 mHz trials, a negligibly small current was observed after the application of seven pulses. In contrast, when using a frequency of 50 mHz, the current increased stepwise in response to each pulse, and a value of approximately 14 nA was obtained after 10 pulses. This current was subsequently maintained without significant deterioration and the τ value was estimated

to be 1872 s. As shown in Fig. 3c, τ increased along with the optical frequency, and the STM–LTM transition was observed at approximately 10 mHz. The associated τ value on the order of 1500 s was maintained above approximately 14 mHz. Thus, an STM–LTM transition could be induced by increasing the optical pulse frequency in addition to increasing the number of pulses.

Figure 3d presents the PPF data for the VG/diamond junctions. This is one of the most common and most important characteristics used to assess synaptic plasticity. This parameter is defined as the ratio of the amplitudes of the (photo)currents induced by the first and second light pulses (A_2/A_1; see the inset to Fig. 3d). The PPF index was found to decrease as the time difference between the first and second pulses (Δt) increased, and decayed based on the double exponential function [19, 33]

$$\frac{A_2}{A_1} = C_1 \cdot exp\left(\frac{-\Delta t}{\tau_1}\right) + C_2 \cdot exp\left(\frac{-\Delta t}{\tau_2}\right) + C_0, \qquad (2)$$

where τ_1 and τ_2 are characteristic relaxation times, C_1 and C_2 are the facilitation magnitudes for rapid and slow decay, and C_0 has a value of 100% (reflecting the fact that the PPF value approaches 100% asymptotically). Fitting the experimental results using Eq. (2) gave τ_1 and τ_2 values of 0.501 and 24.8 s, respectively, which are comparable to the values reported for biological synapses (on the order of milliseconds to seconds) [33-35]. The PPF index was approximately 318% at the minimum Δt value of 1 s, and this value is higher than those reported for optical modulation (in the range of 144 to 204%) [17, 19-21, 36]. The observation of an EPSC, an STM–LTM transition and a reasonable PPF suggest that these VG/diamond junctions are able to function as optoelectronic synapses with photo-sensing properties and optically-controllable synaptic plasticity, and therefore could be used as building blocks for fabricating neuromorphic optical computing devices.

Compared with the other materials, we consider one of the most characteristic features of the VG/diamond junctions is that they have optically-controllable excitatory and inhibitory synaptic characters as shown in Fig. 2(b). In the junctions, potentiation and depression, which correspond to excitatory and inhibitory functions of synapses, are performed optically, bidirectionally and step-by-step, which enables free control of the potentiation states of the carbon artificial synapses. These excitatory and inhibitory synaptic characters are optically tunable and bias polarity to the junctions only determines whether potentiation or depression occurs. In the case for other material systems such as oxide and TMD optoelectronic synapses, depression procedures have to be done by electrically, and optical control is difficult. We think the limitation comes from their working mechanisms [18, 19, 22] and electrical wipe out of carriers is necessary for depression. The working mechanism of our VG/diamond junctions, where redox reaction of graphene/diamond interfaces plays dominant roles, is different from those for other material systems such as oxide and TMD junctions, where optically induced band excitation of semiconductive layers plays dominant roles [18, 19, 22], leading to free optical control of potentiation and depression of the VG/diamond synapses. Also, these functions of the VG/diamond junctions can be translated to produce brain-mimic type image sensing-memory, which would perform stepwise control (increase and decrease) of the color levels (intensity) of each pixel in parallel.

In addition to the optically-controllable excitatory and inhibitory characters of the VG/diamond junctions, there are several other merits for using them as artificial optoelectronic synapses. First, the VG/diamond junctions are composed of common carbon elements and free from rare metals. Contrary, rare metals such as In, Mo, Nb, etc. were necessary for oxide and TMD heterojunctions. Rare metal free characters of the

carbon junctions are one of the most important merits. Second, the carbon junctions have high photoresponsivity with PPF index of 318%, which was higher than those reported for optical modulation (in the range of 144 to 204%). Third, Simple film fabrication process by in-situ CVD and two terminal device structures are also advantageous for the application of the VG/diamond junctions. Most of other artificial synapse needs gate electrodes to tune their electronic characters and they have more complicated three terminal structures. These rare metal-free, highly photosensitive, simple structural characters are superior points of the VG/diamond junctions to other materials, in addition to their optically-controllable excitatory and inhibitory characters.

While evaluating the VG/diamond heterojunctions, variations in optoelectronic memory characteristics were observed, which most likely originated from fluctuations in the fabrication conditions. The key factors that controlled the appearance of the synaptic behavior as well as the optoelectronic and structural properties of the various VG/diamond junctions were therefore examined in detail. Figure 4a plots the normalized conductance values for three typical VG/diamond junctions (samples 1, 2, and 3) over time after irradiation with 10 optical pulses. As a note, growth temperature of the VG layers was set higher (950°C) for sample 1 [24] than those for sample 2 and 3 (900°C). It is apparent that each of these specimens exhibited different photo-memory characteristics. Sample 1, which showed multibit optoelectronic characteristics in a previous study [24], exhibited a negligibly small conductance decay after 10 pulses, while sample 2 (the device used in the present work that showed optoelectronic synaptic behavior) demonstrated an intermediate degree of decay. Sample 3 showed the largest current decay and the lowest photo-responsivity. The relaxation time, τ, was estimated to be 229, 3.57 and 0.0986 min based on fitting the data for samples 1, 2, and 3, respectively, using Eq. (1).

A careful comparison of the Raman spectra for these samples indicated that the I_D/I_G ratio for the samples with a larger conductance decay (samples 2 and 3) was higher, and that τ increased exponentially as the I_D/I_G ratio decreased (Fig. 4b). As discussed earlier in this report, a larger I_D/I_G ratio corresponds to an increase in the proportion of sp^3 defects (most likely due to oxidation of the graphene layers in this case) in graphitic structures. The increase of sp^3 defects by oxidation of graphene layers and/or edge formation would also be expected to increase the interlayer spacing of the VG layers. The interlayer spacing estimated from transmission electron microscopy (TEM) images for a sample fabricated employing the same conditions used to produce sample 2 was 0.37-0.40 nm, which was slightly larger than the range for sample 1 (0.35 to 0.36 nm) (Fig. 4c) [23, 24]. TEM images of the interfaces in sample 2 also indicated a higher concentration of defects and lower crystallinity, which was probably originated from its lower growth temperature, compared with sample 1. Larger interlayer spacing and a greater number of defects of the interfacial graphene layers are believed to increase the oxidation efficiency, and both samples 2 and 3 (which had more defective interfaces) showed rapid conductivity relaxation. Interestingly, Morimoto et al. reported that an increase in the interlayer spacing of graphene layers was an initial and important step in the effective oxidation of graphene [37], which agrees with our proposal that defective interfacial graphene layers are more readily oxidized. These results indicate that controlling the proportion of sp^3 defects in the interfacial graphene layers is vital to fabricating VG/diamond junctions with optoelectronic synaptic characteristics, and sp^3 ratio in the interfacial graphene layers is considered to be controlled by tuning fabrication conditions such as the growth temperature of the VG layers.

Finally, we demonstrated that arrays of these VG/diamond junctions can be used as

image sensors with brain-type optoelectronic memory functions. In these trials, an array with a 2 × 3 structure were fabricated using six VG/diamond junctions (J1 to J6), which showed optoelectronic synaptic functions, and photoirradiation of the array was performed through metal masks with 'I' or 'L' shaped holes (Fig. 5a). The photomemory state of each junction (J1 to J6) was initially reset by continuous irradiation with blue light while applying a negative bias voltage (–10 V) so as to induce the HRS. Following this procedure, the current passing through each junction became negligibly small (< 1 nA at +10 V), confirming a transition to the HRS. Subsequently, intense continuous blue light photoirradiation with a positive bias of +8 V was applied to J1, J2 and J3 in the array through the I-shaped metal mask to obtain LTM states with lower resistance. Continuous blue light irradiation was selected for this purpose to ensure that the memory state of each junction was definitely changed, because of the variations in the photomemory characteristics of the three devices. Following this procedure, J1, J2, J3, and J6 were subjected to low-intensity photoirradiation by applying three optical pulses with a positive bias (using the same irradiation conditions used to generate the data in Fig. 2d) through the L-shaped mask to induce the STM state. During this trial, only junction 6 appeared to show a change in resistance to the STM state, because the resistance states of the junctions 1, 2 and 3 had already changed to the LTM state. As shown in Fig. 2d, the τ value after three pulses was approximately 5 s, which was sufficient to allow measurements of the conductivity of the junctions in the STM state. After these procedures, the current at +2 V (used as an indicator of conductivity) was determined for all six junctions under dark conditions. A relatively small voltage of 2 V was used for these measurements to prevent unexpected changes in the conductivity of the junctions. Figures 5b, 5c and 5d present maps of the current values for the junctions (J1 to J6) after

0 min (immediately after the start of photoirradiation), 1 min and 20 min after photoirradiation. Here, the magnitude of the current is expressed on a gray scale with brighter or darker colors corresponding to lower or higher current values, which correspond to conductivity of the junctions, respectively. At 0 min (Fig. 5b), the map shows junctions J1, J2 and J3 as solid black, meaning that they were in the LRS, while J4 and J5 are white and J6 is gray color, meaning that J4 and J5 were in the HRS and J6 was in an intermediate state (with a slightly higher conductivity than those in HRS). Thus, the map reflects the irradiation through the L-shaped mask, although the color of the J6 portion is much lighter than that in the J1, J2 and J3 regions because J6 received only weak irradiation. It is evident from these data that only the resistance states of the photo-irradiated junctions were changed and memorized based on changes in the magnitude of the resistance values, and so the VG/diamond array behaved as an image sensor with a photo-memory function. In the map for the array after 1 min (Fig. 5c), J6 is white, indicating a change to the HRS and also that the information captured by this junction in the STM state was lost within a short time span. In contrast, the J1, J2 and J3 regions retain a black color in the map even after 20 min (Fig. 5d), meaning that the LRS of these junctions was retained for this time span. The maps for the array after 1 and 20 min show an I-shaped black portion, corresponding to the intense photo-irradiation through the I-shaped mask. This I-shaped image remained for a prolonged time because the LTM state had been imparted to the three junctions by the strong photoirradiation. These results confirm that the memory retention time for a VG/diamond array can be controlled by tuning the optical stimulation intensity (that is, the number of optical pulses, frequency, etc.), and so these devices could be used as novel image sensors, in which information given through weakly stimuli (that being of low interest) is lost immediately and only

important information given through strongly stimuli (that being of high interest) is retained optoelectronically. Such image sensors could be operated at high speed regardless of the number of junctions in the array because the information is memorized simultaneously by all junctions by massively parallel characters of light. These features of the VG/diamond junctions are expected to permit the development of novel high-speed image sensing-memory units (that is, image sensors with photomemory functions) capable of screening information depending on its importance, which is considered to be a requirement for edge computing in the near future. The present demonstration was performed using a small, primitive array of six junctions but is sufficient to demonstrate the fundamental image sensing-memory concept. We believe that the future development of this concept could lead to the production of practical image sensors with brain-mimicking memory functions based on the larger-scale integration of these VG/diamond junctions.

4. Conclusions

This work is first demonstration of optoelectronic synaptic characters of carbon heterojunctions such as graphene/diamond junctions with their possible working mechanism and their use as novel image sensors with brain-mimic optoelectronic memory functions. The VG/diamond devices exhibited an optically controllable EPSC, an STM-LTM transition and PPF properties, all of which are fundamental aspects of the functioning of the human brain. A high PPF index (greater than 300%) was observed, which is the highest value yet obtained by optical modulation. In addition to their optically-controllable excitatory and inhibitory characters, rare metal-free, highly photosensitive, simple structural characters are superior points of the VG/diamond

junctions to other materials. We consider the difference of working mechanism between the VG/diamond junctions and other synaptic junctions leads to superior optoelectronic features such as optically-controllable excitatory and inhibitory characters, and higher PPF of the junctions. A careful analysis of the optoelectronic and structural characteristics of the various junctions showed that control of the proportion of sp^3 components in the interfacial graphene layers is a key factor in fabricating junctions with optoelectronic synaptic characteristics. We also found that these VG/diamond arrays could be used as image sensing-memory devices capable of selecting information depending on its importance, which is thought to be necessary for next-generation computing.

Acknowledgements

This work was partly supported by JSPS KAKENHI Grant Number 21H01388, by Sumitomo Electric Industries group CSR foundation, and Iketani Science and Technology Foundation.

References

[1] Q Xia, and J. J. Yang, Memristive crossbar arrays for brain-inspired computing, Nature Mater. 18 (2019) 309-323.

[2] Y. Chen, H. Li, C. Wu, C. Song, S. Li, C. Min, et al., Neuromorphic computing's yesterday, today, and tomorrow–an evolutional view, Integ. VLSI J. 61 (2018) 49-61.

[3] D. Ielmini and S. Ambrogio, Emerging neuromorphic devices, Nanotechnology 31 (2020) 092001-1-24.

[4] M. Lee, W. Lee S. Choi, J-W. Jo, J. Kim, S. K. Park, et al., Brain-Inspired Photonic Neuromorphic Devices using Photodynamic Amorphous Oxide Semiconductors and their Persistent Photoconductivity, Adv. Mater. 29 (2017) 1700951-1-8.

[5] S. Dai, Y. Zhao, Y. Wang, J. Zhang, L. Fang, S. Jin, et al., Recent Advances in Transistor-Based Artificial Synapses, Adv. Funct. Mater. 29 (2019) 1903700-1-22.

[6] S. L. Barbera, D. R. B. Ly, G. Navarro, N. Castellani, O. Cueto, G. Bourgeois, et al., Narrow Heater Bottom Electrode-Based Phase Change Memory as a Bidirectional Artificial Synapse, Adv. Electron. Mater., 4 (2018) 1800223-1-8.

[7] Y. V. Pershin, and M. D. Ventra, Memory effects in complex materials and nanoscale systems, Advances in Physics 60 (2011) 145-227.

[8] T. Chang, S-H. Jo, and W. Lu, Short-Term Memory to Long-Term Memory Transition in a Nanoscale Memristor, ACS nano, 5 (2011) 7669-7676.

[9] S. H. Jo, T. Chang, I. Ebong, B. B. Bhadviya, P. Mazumder, and W. Lu, Nanoscale Memristor Device as Synapse in Neuromorphic Systems, Nano Lett. 10 (2010) 1297-1301.

[10] T-H. Lee, H-G. Hwang, J-U. Woo, D-H. Kim, T-W. Kim, and S. Nahm, Synaptic Plasticity and Metaplasticity of Biological Synapse Realized in a $KNbO_3$ Memristor for

Application to Artificial Synapse, ACS Appl. Mater. Interfaces 10 (2018) 25673-25682.

[11] W. Wang, G. N. Panin, X. Fu, L. Zhang, P. IIanchezhiyan, V. O. Pelenovich, et al., MoS_2 memristor with photoresistive switching, Sci. rep. 6 (2016) 31224-1-10.

[12] P. Maier, F. Hartmann, M. R. S. Dias, M. Emmerling, C. Schneider, L. K. Castelano, et al., Light sensitive memristor with bi-directional and wavelength-dependent conductance control, Appl. Phys. Lett. 109, (2016) 023501-1-5.

[13] R. Basori, K. Das, P. Kumar, K. S. Narayan, and A. K. Raychaudhuri, Large photoresponse of Cu:7,7,8,8-tetracyanoquinodimethane nanowire arrays formed as aligned nanobridges, Appl. Phys. Lett. 102 (2013) 061111-1-4.

[14] K. Ueda, S. Aichi and H. Asano, Photo-controllable memristive behavior of graphene/diamond heterojunctions, Appl. Phys. Lett., 108 (2016) 222102-1-5.

[15] L. Hu, J. Yang, J. Wang, P. Cheng, L. O. Chua, and F. Zhuge, All-Optically Controlled Memristor for Optoelectronic Neuromorphic Computing, Adv. Funct. Mater. 31 (2021) 2005582-1-10.

[16] M. Lee, W. Lee, S. Choi, J-W. Jo, J. Kim, S. K. Park, et al., Brain-Inspired Photonic Neuromorphic Devices using Photodynamic Amorphous Oxide Semiconductors and their Persistent Photoconductivity, Adv. Mater. 29 (2017) 1700951-1-8.

[17] S. Gao, G. Liu, H. Yang, C. Hu, Q. Chen, G. Gong, et al., An Oxide Schottky Junction Artificial Optoelectronic Synapse, ACS Nano 13 (2019) 2634-2642.

[18] J. Sun, S. Oh, Y. Choi, S. Seo, M. J. Oh, M. Lee, et al., Optoelectronic Synapse Based on IGZO-Alkylated Graphene Oxide Hybrid Structure, Adv. Funct. Mater. 28 (2018) 1804397-1-9.

[19] S. Wang, C. Chen, Z. Yu, Y. He, X. Chen, Q. Wan, et al., A MoS_2/PTCDA Hybrid Heterojunction Synapse with Efficient Photoelectric Dual Modulation and Versatility,

Adv. Mater. 31 (2019) 1806227-1-9.

[20] M. M. Islam, D. Dev, A. Krishnaprasad, L. Tetard, and T. Roy, Optoelectronic synapse using monolayer MoS_2 field effect transistors, Sci. Rep. 10 (2020) 21870-1-9.

[21] L. Yin, W. Huang, R. Xiao, W. Peng, Y. Zhu, Y. Zhang, et al., Optically Stimulated Synaptic Devices Based on the Hybrid Structure of Silicon Nanomembrane and Perovskite, Nano Lett. 20 (2020) 3378-3387.

[22] J. Zhang, S. Dai, Y. Zhao, J. Zhang, and J. Huan, Recent Progress in Photonic Synapses for Neuromorphic Systems, Adv. Intell. Syst. 2 (2020) 1900136-1-17.

[23] K. Ueda, H. Itou and H. Asano, Photomemristors using carbon nanowall/diamond heterojunctions, J. Mater. Res., 34 (2019) 626-633.

[24] K. Ueda, Y. Mizuno and H. Asano, Multibit optoelectronic memory using graphene/diamond (carbon sp^2-sp^3) heterojunctions and its arithmetic functions, Appl. Phys. Lett., 117 (2020) 092103-1-5.

[25] K. Ueda, K. Kawamoto, T. Soumiya and H. Asano, High-temperature characteristics of Ag and Ni/diamond Schottky diodes, Dia. Relat. Mater., 38 (2013) 41-44.

[26] G. Eda, and M. Chhowalla, Chemically Derived Graphene Oxide: Towards Large-Area Thin-Film Electronics and Optoelectronics, Adv. Mater. 22 (2010) 2392-2415.

[27] L. M. Malard, M. A. Pimenta, G. Dresselhaus, and M. S. Dresselhaus, Raman spectroscopy in graphene, Phys. Rep., 473 (2009) 51-87.

[28] S. Kondo, S. Kawai, W. Takeuchi, K. Yamakawa, S. Den, H. Kano, et al., Initial growth process of carbon nanowalls synthesized by radical injection plasma-enhanced chemical vapor deposition, J. Appl. Phys., 106 (2009) 094302-1-6.

[29] R. J. Nemanich, J. T. Glass, G. Lucovsky, and R. E. Shroder, Raman scattering characterization of carbon bonding in diamond and diamondlike thin films, J. Vac. Sci. Tech. A, 6 (1988) 1783-1787.

[30] S. G. Hu, Y. Liu, T. P. Chen, Z. Liu, Q. Yu, L. J. Deng, et al., Emulating the Ebbinghaus forgetting curve of the human brain with a NiO-based memristor, Appl. Phys. Lett. 103 (2013) 133701-1-4.

[31] D. C. Rubin, and A. E. Wenzel, One hundred years of forgetting: A quantitative description of retention, Psychol. Rev. 103 (1996) 734-760.

[32] J. L. McGaugh, Memory--a Century of Consolidation, Science 287 (2000) 248-251.

[33] R. S. Zucker, and W. G. Regehr, Annu. Short-Term Synaptic Plasticity, Rev. Physiol. 64 (2002) 355-405.

[34] C. S. Yang, D. S. Shang, N. Liu, G. Shi, X. Shen, R. Cheng et al., A Synaptic Transistor based on Quasi-2D Molybdenum Oxide, Adv. Mater. 29 (2017) 1700906-1-10.

[35] C. Du, W. Ma, T. Chang, P. Sheridan, and W. D. Lu, Biorealistic Implementation of Synaptic Functions with Oxide Memristors through Internal Ionic Dynamics, Adv. Funct. Mater. 25 (2015) 4290-4299.

[36] F. Ma, Y. Zhu, Z. Xu, Y. Liu, X. Zheng, S. Ju, et al., Optoelectronic Perovskite Synapses for Neuromorphic Computing, Adv. Funct. Mater. 30 (2020) 1908901-1-9.

[37] N. Morimoto, H. Suzuki, Y. Takeuchi, S. Kawaguchi, M. Kunisu, C. W. Bielawski et al., Real-Time, in Situ Monitoring of the Oxidation of Graphite: Lessons Learned, Chem Mater. 29 (2017) 2150-2156.

Figure captions

Figure 1. a) Current-voltage characteristics of the VG/diamond junctions in response to photoirradiation at the maximum voltage (±8 V) for approximately 10 s. b) Current-voltage characteristics of the junctions in HRS or LRS measured in dark conditions. c) Current retention properties of the junctions. The inset presents a diagram of a junction, showing that the current passes through sp^2-sp^3 carbon interfaces. d) Illustrations summarizing the working principles of a VG/diamond junction under photoirradiation in conjunction with the application of negative (left) and positive (right) bias voltages. e) Raman spectra obtained from the VG/diamond junction in the LRS and HRS.

Figure 2. a) The effects of optical pulses on the junction current at a bias voltage of +8 V, applying 10 optical pulses with a light intensity of 78 μW/cm^2 and pulse width of 50 ms at a frequency of 0.2 Hz. The inset shows the effect of the number of pulses on the current at various light frequencies. b) The excitatory post-synaptic current (EPSC) as a function of the number of optical pulses in conjunction with a negative bias voltage. The effect of the number of optical pulses on c) the conductance decay (using 3 or 12 pulses) and d) the junction relaxation time, τ. The dotted lines in Fig. 2c are fitting results using eq. (1).

Figure 3. The junction current over time during photoirradiation with an optical pulse frequency of a) 2 and b) 50 mHz. c) The effect of pulse frequency on the junction relaxation time, τ (optical pulses; 78 μW/cm^2, 50 ms). d) The paired pulse facilitation (PPF) index as a function of the time span (Δt) between the first and second pulses applied to the VG/diamond junction. The dotted line is the fitting result using eq. (2).

Figure 4. a) The time dependence of the normalized conductance values for three typical junctions (samples 1, 2 and 3) after photoirradiation using 10 optical pulses (38 μW/cm^2, 50 ms). The dotted lines are fitting results using eq. (1). b) The correlation between the I_D/I_G ratio and the relaxation time, τ. c) TEM images for the VG/diamond junctions fabricating in the same conditions with sample 2 (left) and sample 1 (right).

Figure 5. a) Diagrams summarizing the photoirradiation experiments performed with a 2 × 3 VG/diamond arrays using six junctions (J1 to J6). The array was subjected to intense or weak photoirradiation performed sequentially through metal masks having ‘I’ or ‘L’ shaped holes. Mapping images of the current values obtained for the VG/diamond array with six junctions at b) 0 min (that is, immediately after the onset of photoirradiation), c) 1 min and d) 20 min after photoirradiation. The blue lines are visual guides showing the photoirradiated regions. The ‘L’ and ‘I’ characters were optoelectronically memorized by the array.

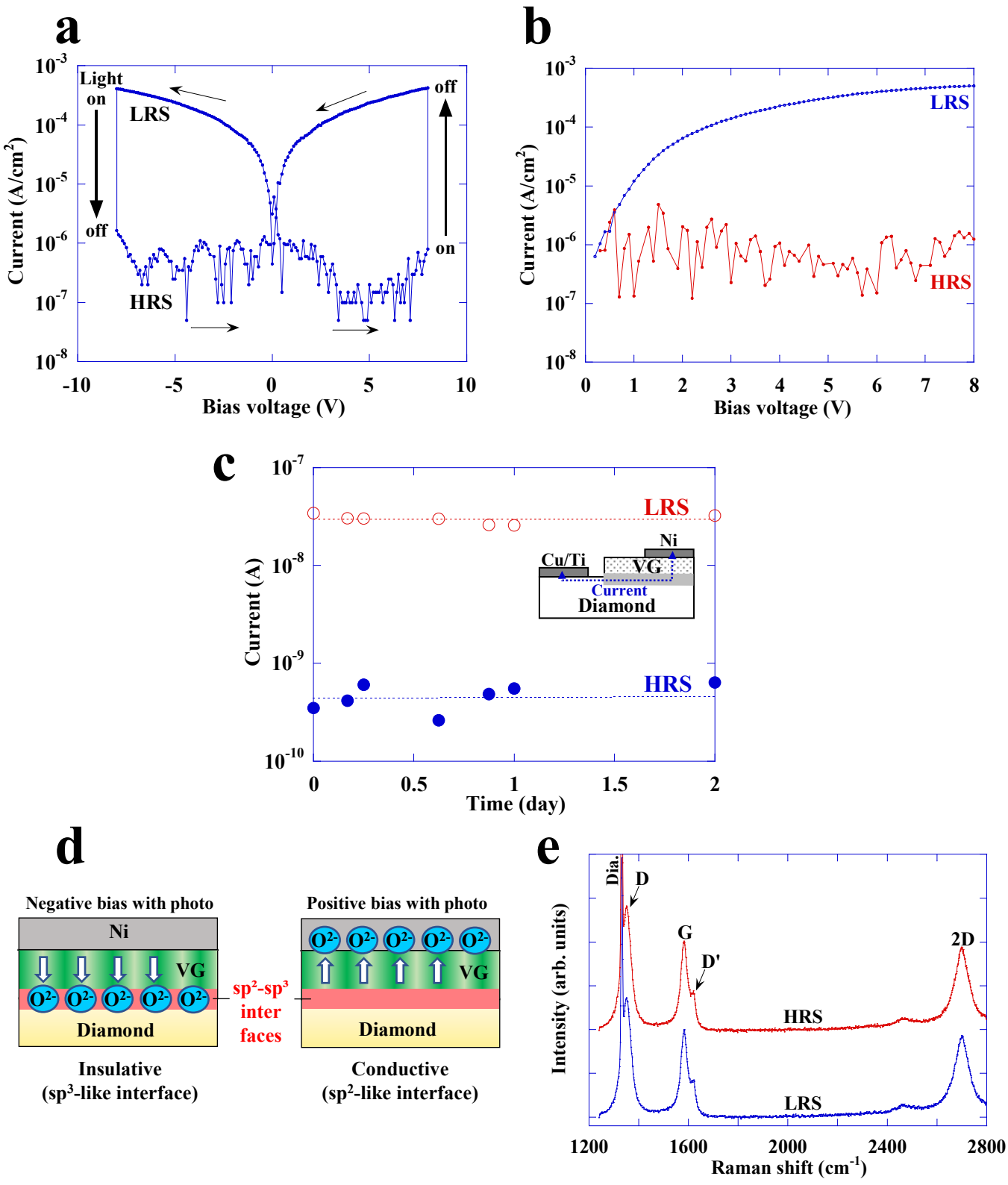

Figure 1. a) Current-voltage characteristics of the VG/diamond junctions in response to photoirradiation at the maximum voltage (±8 V) for approximately 10 s. b) Current-voltage characteristics of the junctions in HRS or LRS measured in dark conditions. c) Current retention properties of the junctions. The inset presents a diagram of a junction, showing that the current passes through sp^2-sp^3 carbon interfaces. c) Illustrations summarizing the working principles of a VG/diamond junction under photoirradiation in conjunction with the application of negative (left) and positive (right) bias voltages. d) Raman spectra obtained from the VG/diamond junction in the LRS and HRS.

Fig. 1

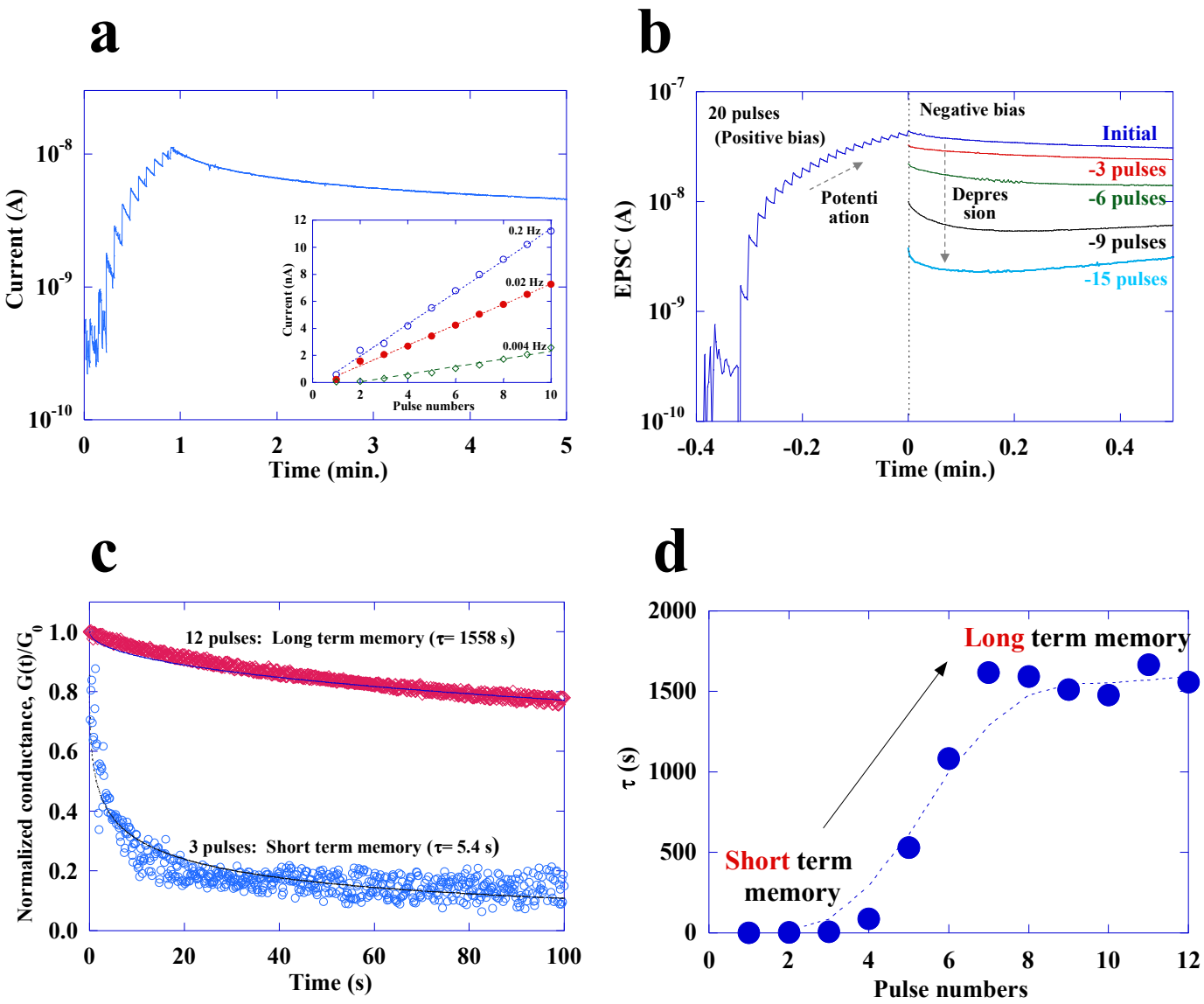

Figure 2. a) The effects of optical pulses on the junction current at a bias voltage of +8 V, applying 10 optical pulses with a light intensity of 78 μW/cm^2 and pulse width of 50 ms at a frequency of 0.2 Hz. The inset shows the effect of the number of pulses on the current at various light frequencies. b) The excitatory post-synaptic current (EPSC) as a function of the number of optical pulses in conjunction with a negative bias voltage. The effect of the number of optical pulses on c) the conductance decay (using 3 or 12 pulses) and d) the junction relaxation time, τ. The dotted lines in Fig. 2c are fitting results using eq. (1).

Fig. 2

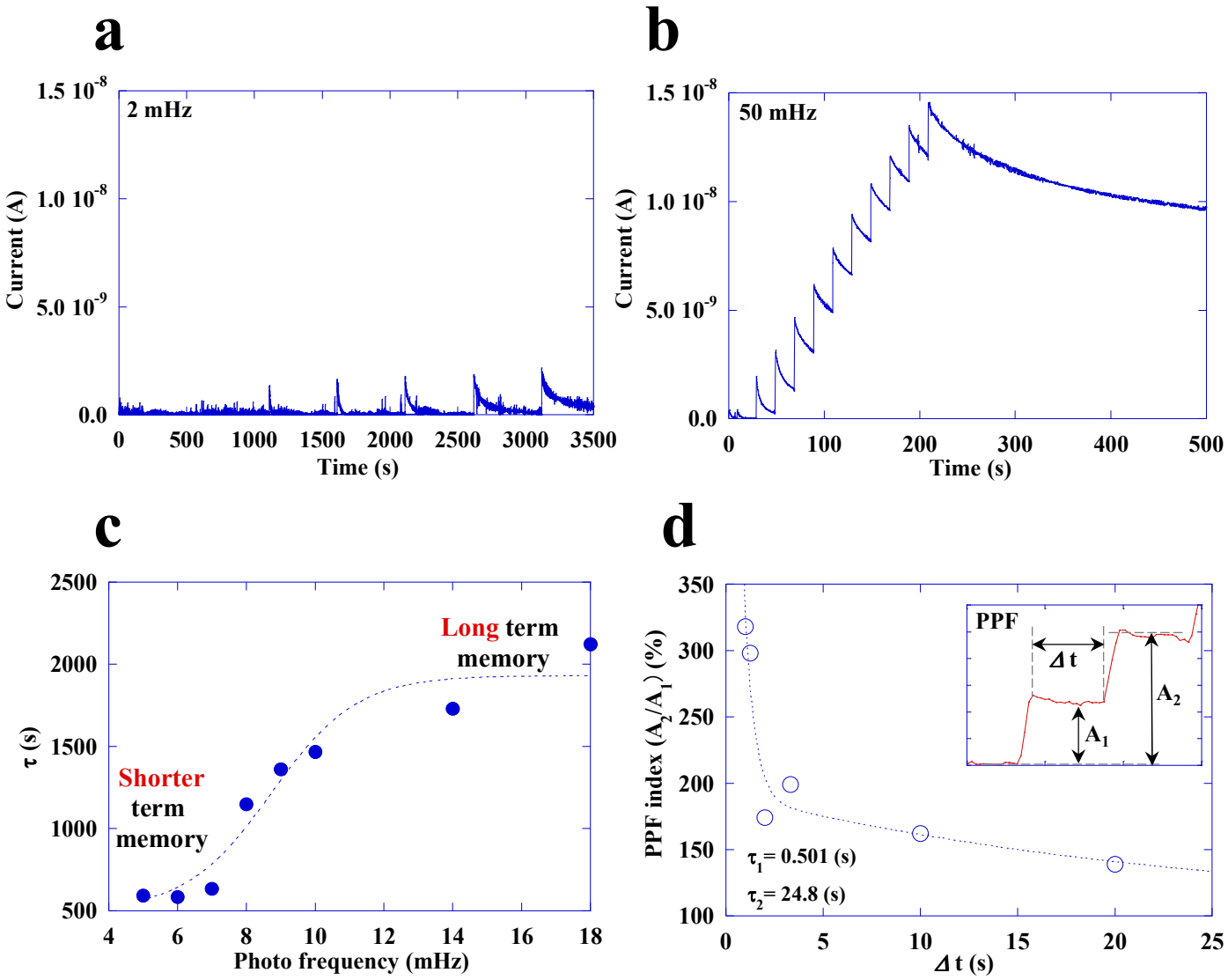

Figure 3. The junction current over time during photoirradiation with an optical pulse frequency of a) 2 and b) 50 mHz. c) The effect of pulse frequency on the junction relaxation time, τ (optical pulses; 78 μW/cm^2, 50 ms). d) The paired pulse facilitation (PPF) index as a function of the time span (Δt) between the first and second pulses applied to the VG/diamond junction. The dotted line is the fitting result using eq. (2).

Fig. 3

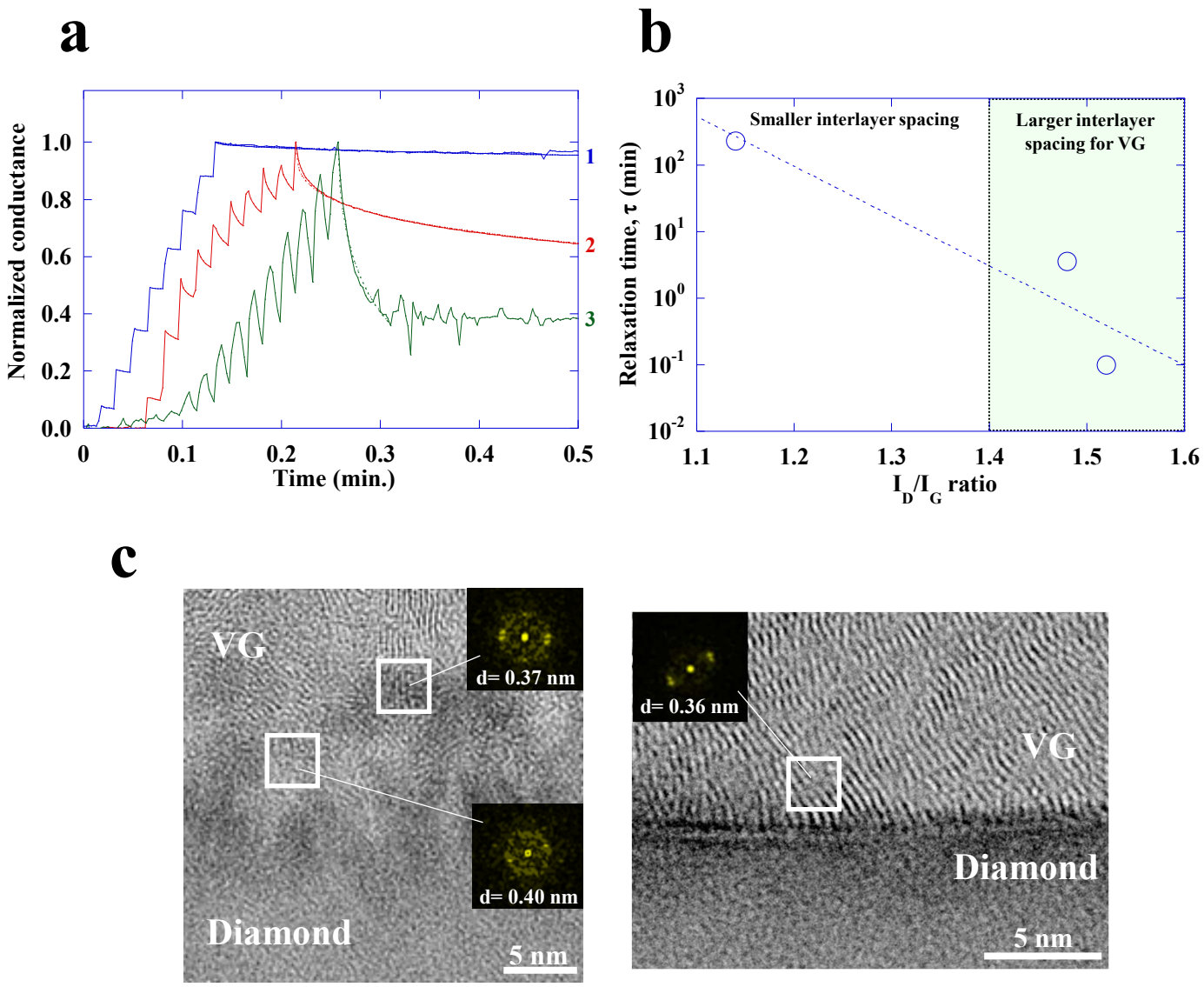

Figure 4. a) The time dependence of the normalized conductance values for three typical junctions (samples 1, 2 and 3) after photoirradiation using 10 optical pulses (38 μW/cm^2, 50 ms). The dotted lines are fitting results using eq. (1). b) The correlation between the I_D/I_G ratio and the relaxation time, τ. c) TEM images for the VG/diamond junctions fabricating in the same conditions with sample 2 (left) and sample 1 (right).

Fig. 4

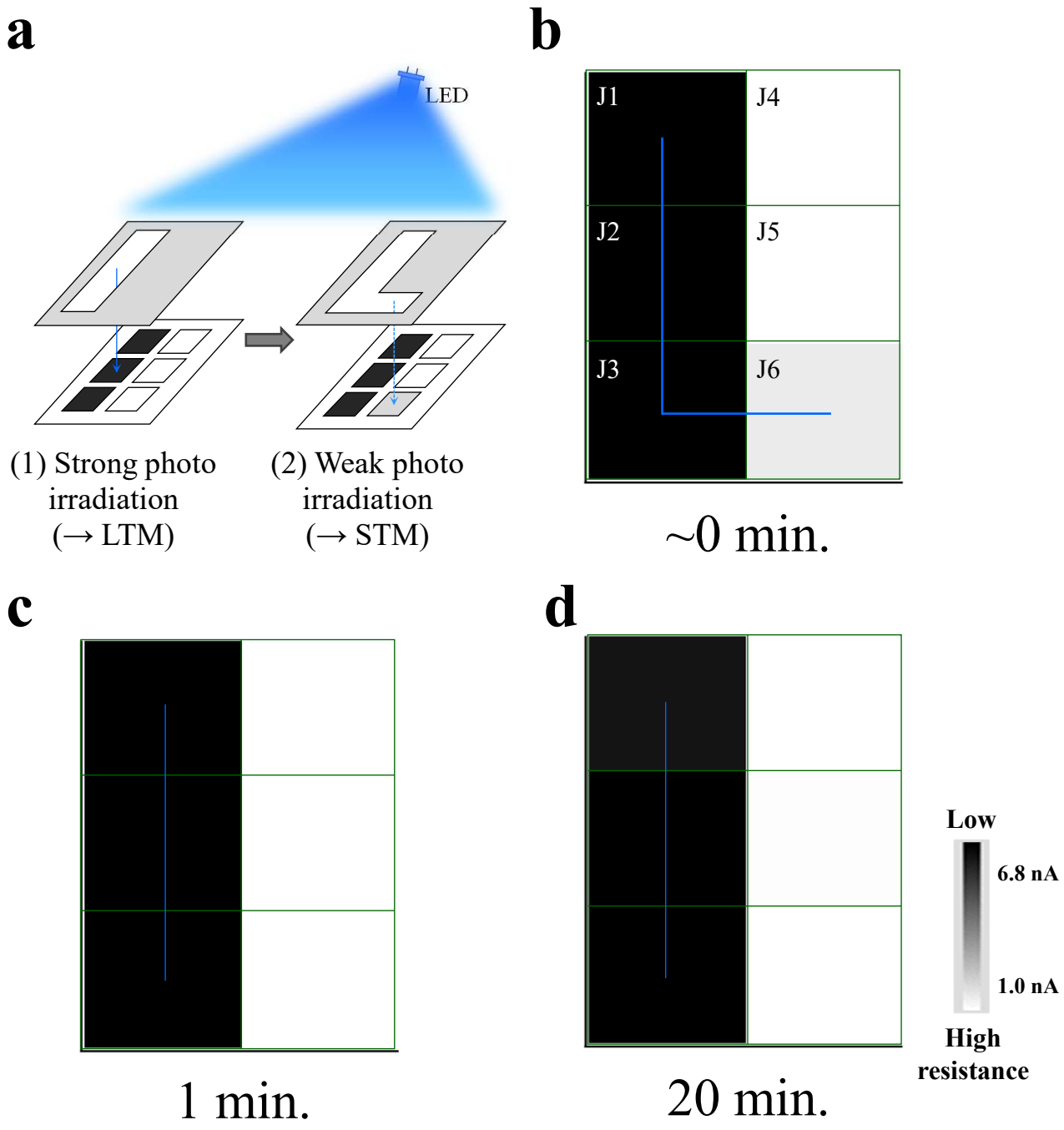

Figure 5. a) Diagrams summarizing the photoirradiation experiments performed with a 2 × 3 VG/diamond arrays using six junctions (J1 to J6). The array was subjected to intense or weak photoirradiation performed sequentially through metal masks having 'I' or 'L' shaped holes. Mapping images of the current values obtained for the VG/diamond array with six junctions at b) 0 min (that is, immediately after the onset of photoirradiation), c) 1 min and d) 20 min after photoirradiation. The blue lines are visual guides showing the photoirradiated regions. The 'L' and 'I' characters were optoelectronically memorized by the array.

Fig. 5